

## Article

# Multiple Exciton Generation Solar Cells: Numerical Approaches of Quantum Yield Extraction and Its Limiting Efficiencies

Jongwon Lee <sup>1</sup>  and Chi-Hyung Ahn <sup>2,\*</sup> <sup>1</sup> KOMICO, Anseong 17567, Gyeonggi-do, Republic of Korea<sup>2</sup> School of Electrical, Electronics and Communication Engineering, Korea University of Technology and Education, Cheonan-si 31253, Chungcheongnam-do, Republic of Korea

\* Correspondence: chahn@koreatech.ac.kr

**Abstract:** Multiple exciton generation solar cells exhibit low power conversion efficiency owing to non-radiative recombination, even after the generation of numerous electron and hole pairs per incident photon. This paper elucidates the non-idealities of multiple exciton generation solar cells. Accordingly, we present mathematical approaches for determining the quantum yield to discuss the non-idealities of multiple exciton generation solar cells by adjusting the delta function. We present the use of the Gaussian distribution function to present the occupancy status of carriers at each energy state using the Dirac delta function. Further, we obtained ideal and non-ideal quantum yields by modifying the Gaussian distribution function for each energy state. On the basis of this approach, we discuss the material imperfections of multiple exciton generations by analyzing the mathematically obtained quantum yields. Then, we discuss the status of radiative recombination calculated from the ratio of radiative to non-radiative recombination. Finally, we present the application of this approach to the detailed balance limit of the multiple exciton generation solar cell to evaluate the practical limit of multiple exciton generation solar cells.

**Keywords:** multiple exciton generation; quantum yield; thermodynamic limit; detail balance limit



**Citation:** Lee, J.; Ahn, C.-H. Multiple Exciton Generation Solar Cells: Numerical Approaches of Quantum Yield Extraction and Its Limiting Efficiencies. *Energies* **2023**, *16*, 993. <https://doi.org/10.3390/en16020993>

Academic Editor: Abasifreke Ebong

Received: 27 November 2022

Revised: 4 January 2023

Accepted: 10 January 2023

Published: 16 January 2023



**Copyright:** © 2023 by the authors. Licensee MDPI, Basel, Switzerland. This article is an open access article distributed under the terms and conditions of the Creative Commons Attribution (CC BY) license (<https://creativecommons.org/licenses/by/4.0/>).

## 1. Introduction

Enhancement of power conversion efficiency is essential for photovoltaic (PV) devices. Various concepts have been realized to date to surpass the Shockley–Queisser (SQ) limit, such as tandem (multi-junction) solar cells, multiple exciton generation, intermediate bands, and metallic nano-concepts (plasmonic) [1–5].

Multiple exciton generation solar cells (MEGSCs) are promising PV devices that surpass the SQ limit [1,2]. Ideally, one incident photon with an energy ( $E_{ph}$ ) greater than the bandgap energy ( $E_g$ ) can generate multiple electron-hole pairs (EHPs), where excess energy ( $E_{ph}-E_g$ ) contributes to the creation of additional EHPs by impact ionization [2,3]. The number of generated and recombined EHPs should be conserved under the conditions of substantial blackbody radiation. Since Kolondinski et al. [6] first reported the multiple exciton generation (MEG) effect with internal quantum efficiency (IQE) of over 100% at 3.4 eV in Si solar cells, where the excess energy of ultraviolet radiation created hot carriers via impact ionization, the advanced theoretical research proposed the use of nanostructures (e.g., quantum dots) owing to their excellent quantum confinement. Quantum efficiency is the ratio of the number of charges collected by the solar cell to the incoming or absorbed photon energy. Typically, the IQE relies on the absorption of light to create EHP. Bulk Silicon has an indirect transition from  $\Gamma$  point to X point (~1.12 eV) and a direct transition  $\Gamma$  point (~3.4 eV) due to an indirect bandgap material. The IQE over 100% occurred at  $\Gamma$  point, as the absorbed photon energy (more than 3.4 eV, the near ultraviolet region) and its excess energy ( $3.4 - 1.12 = 2.28$  eV) could create another hot carrier by impact ionization [3,6]. Furthermore, various studies reported the efficiency limit of MEG and the possibility of

its occurrence in nanostructures based on the quantum yield (QY) and threshold energy ( $E_{th}$ ) [7–14]. Notably, the QY and  $E_{th}$  are critical parameters that determine the ideality of MEGSCs [12,13].  $E_{th}$  refers to the photon energy at which the QY exceeds 100%. In theory, ideal QY (IQY) increases in accordance with a staircase (step) function. However, the experimental QY data deviate from the ideal case: QY increases linearly after  $E_{th}$  [12–21]. More specifically, the QY can show the loss of carriers corresponding to each energy state in quantum dot structures, depending on the material properties (ex. surface states) [16–21]. The non-ideal QY (NQY) was experimentally extracted using pump-probe measurements by comparing the peaks corresponding to the excited and ground states [12,13,16–21]. Moreover, it was modeled theoretically using the MEG efficiency ( $E_g$ /the additional energy required to create further EHPs) for the slope calculation of NQY. Additionally,  $E_{th}$  has been defined in terms of the effective mass and MEG efficiency [21,22]. Furthermore, NQY and its theoretical efficiency limit have been extensively studied [12,13,16–18,23–28]. However, most experimental data depend on specific materials, and the QY cannot be generalized [15].

First, this paper discusses the Dirac delta function and unit step function based on their mathematical relationship. The integration of the Heaviside unit step function under a shift of  $m \cdot E_g$  results in IQY, and its derivative yields a group of delta functions. Furthermore, the deviation exhibited by the delta function can describe NQY [29,30]. Most QY extractions are performed by fitting certain parameters from the experimental results [12,13,16–20]. In contrast, this study employed a purely theoretical approach by adjusting the delta function to obtain both IQY and NQY and analyzed the non-idealities of MEGSCs. These aspects have not been thoroughly addressed in the previous research. NQY is a good indicator of the material status in quantum dot MEGSCs, as it includes material information. Even though substantial QY can be achieved experimentally, it will be difficult to implement efficient MEGSCs without a near-perfect solar cell material [31]. The conventional detailed balance (DB) limit considers only one radiative recombination to predict the maximum theoretical efficiency limit. However, NQY includes material information such as non-radiative recombination (NR: Auger recombination, surface defects, and phonons) and describes the loss of carriers, incomplete light absorption, incomplete photo-generated current, and its low practical efficiency [31–35]. Thus, we use the proposed QY extraction method in the DB limit of MEGSC to predict higher practical efficiency limit by comparing peak intensities (maximum peak at  $E_g$  and second maximum peak at  $2E_g$ ) while considering the NR impact. This approach is similar to QY extraction by pump-probe measurement because of the comparison of the peak intensities. However, this QY extraction approach explains the carrier occupancy rate at each energy state, where a low occupancy rate indicates carrier loss owing to non-radiative recombination, incomplete light absorption, and insufficient photo-generated current [35]. In other words, the ratio of the peak intensities describe the status of radiative recombination, including NR and its correlated ideal reverse saturation current density. Therefore, the variation in the ideal saturation current can determine the performance of the MEGSC.

## 2. Theory

We applied mathematical approaches to derive a generalized QY. In theory, the derivative of the unit step function is a Dirac delta function. Thus, the staircase function can be expressed as follows [30,36]:

$$IQY = H(E - E_g) + H(E - 2 \cdot E_g) + \dots + H(E - m \cdot E_g) + \dots + H(E - M \cdot E_g) \quad (1)$$

where  $H$  denotes the Heaviside step function,  $m$  is a positive integer.

Furthermore, the derivative of each step function is

$$\delta = [\delta(E - E_g), \delta(E - 2 \cdot E_g), \dots, \delta(E - m \cdot E_g), \dots, \delta(E - M \cdot E_g)], \quad (2)$$

where  $\delta$  denotes the delta function.

For this simulation, we assumed that if multiple electrons corresponding to each energy state  $m \cdot E_g$  certainly exist, the Dirac delta function at  $m \cdot E_g$  can represent the occupancy status of electrons to exhibit ideal qualities. To demonstrate the delta functions, we employed a Gaussian distribution function (GDF), as expressed in Equation (3), primarily because the delta function can represent a form of the GDF limit. The GDF is the probability density function of a normal distribution. In the limit form of the GDF case, the delta function presents a high probability density; otherwise, it displays a low probability density. We set the mean or expected value of the variable to correspond to the distribution shown in Equation (3) as  $m \cdot E_g$ , to represent multiple energy states.

$$f(E) = \frac{1}{\sigma\sqrt{2\pi}} e^{-\frac{1}{2} \cdot \left(\frac{E - m \cdot E_g}{\sigma}\right)^2}, \quad (3)$$

where  $\sigma$  indicates the standard deviation ( $=0.004, 0.1, 0.2, 0.3, 0.4, 0.5 \dots$ ),  $E$  represents an arbitrary energy,  $E_g$  denotes the bandgap energy, and  $m = 1, 2, 3, \dots$ .

First, we calculated the GDF at  $m \cdot E_g$ , where  $m = 1, 2, 3 \dots$  (from Equations (3)–(5)) to obtain the Dirac delta function corresponding to each energy state as follows:  $f_1(E)$  is the GDF at  $E_g$  corresponding to the generation of one EHP. Following that, we employed cumulative integration and normalized the value of  $E$  (Equation (5)) for each energy state. Finally, we added the values to obtain the QY (Equation (7)). Figure 1 illustrates the procedure for IQY. Figures 2 and 3 represent the procedure for NQY.

$$f_1(E) = \frac{1}{\sigma_1\sqrt{2\pi}} e^{-\frac{1}{2} \cdot \left(\frac{E - E_g}{\sigma_1}\right)^2} \quad (4)$$

$$f_m(E) = [f_1(E), \frac{1}{\sigma_2\sqrt{2\pi}} e^{-\frac{1}{2} \cdot \left(\frac{E - 2 \cdot E_g}{\sigma_2}\right)^2}, \frac{1}{\sigma_3\sqrt{2\pi}} e^{-\frac{1}{2} \cdot \left(\frac{E - 3 \cdot E_g}{\sigma_3}\right)^2}, \dots] / f_1(E) \quad (5)$$

$$f_n(E) = \left[ \frac{\sum_{i=1}^n \int_{E_i=0\text{eV}}^{x_n} f_1(E) dE}{\int_{E_i=0\text{eV}}^{E_f=10\text{eV}} f_1(E) dE}, \frac{\sum_{i=1}^n \int_{E_i=0\text{eV}}^{x_n} \frac{1}{\sigma_2\sqrt{2\pi}} e^{-\frac{1}{2} \cdot \left(\frac{E - 2 \cdot E_g}{\sigma_2}\right)^2} dE}{\int_{E_i=0\text{eV}}^{E_f=10\text{eV}} f_1(E) dE}, \dots \right] \quad (6)$$

$$\text{IQY} = \text{sum}(f_n(E)), \quad (7)$$

where  $f_1$  indicates the GDF at  $E_g$ ,  $f_m(E)$  indicates GDF at  $m \cdot E_g$ ,  $-\infty < x_n < \infty$ ,  $\sigma$  denotes the standard deviation corresponding to the energy state ( $=m \cdot E_g$ ),  $m = 1, 2, 3 \dots$ , and  $f_n$  represents the calculation of the unit-step function from  $f_m$  (Equation (3)) at each energy state.  $E_i$  indicates the initial energy state,  $E_f$  indicates the final energy state, and  $x_n$  is 0.01, 0.02,  $\dots$ , 10 eV.

As  $\sigma$  decreases, the GDF exhibits a very sharp peak, like a delta function. By contrast, increasing  $\sigma$  increases the width and lowers the peak of the GDF distribution. Therefore, the deviation from the ideal condition (i.e., the non-ideal condition) can be effectively determined by varying  $\sigma$ . Therefore, we chose a small value of  $\sigma$  and a high peak at  $E_g$  to explain the generation of one EHP. Subsequent integration of each delta function yields the unit step function for each energy state. Finally, the cumulative sum of each step function yields the IQY.

For the value of  $\sigma$  for each energy state, we referred to the value of the external radiative recombination efficiency (the ratio of radiative to non-radiative recombination). The fraction of radiative recombination,  $f_C$ , can be considered to determine the peak intensity corresponding to each energy state [1,37,38]. A small external radiative efficiency (ERE) or  $f_C$ , such as  $10^{-5}$ – $10^{-10}$ , indicates a high non-radiative recombination rate, which results in a low power conversion efficiency [37]. Thus, we set the ratio of the second to first peak to represent the non-radiative recombination rate.

For IQY, we assumed  $\sigma$  to be  $4 \times 10^{-3}$  and normalized at each energy state, such as the delta function in a zero-dimensional structure (see Figure 1a and Equation (5)). The normalized cumulative integration of this function yields an individual step function for each state (Figure 1b, Equation (6)), and the summation of each step function yields: the staircase function (Figure 1c, Equation (7)). By contrast, NQY has an increased  $E_{th}$  and a different shape in the QY curve. The increase in  $E_{th}$  necessitates a higher photon energy to generate multiple EHPs.

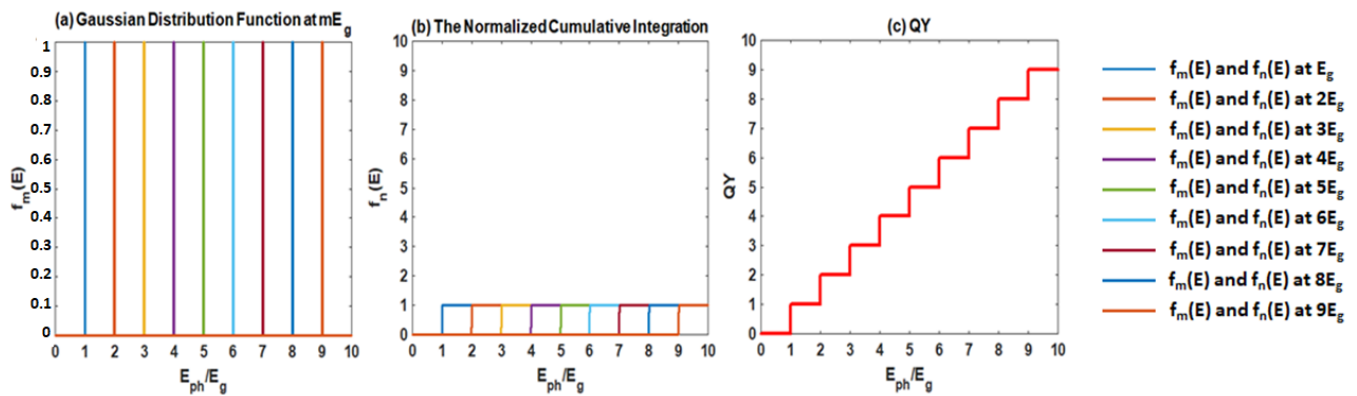


**Figure 1.** Conversion from the Gaussian distribution function to the IQY. (a) The delta function by normalized GDF of each energy state, (b) the step function of each energy state, and (c) the corresponding QYs. The units are arbitrary for (a–c) [Reprinted/Adapted from Ref. [39], 2021, Jongwon Lee, CC BY 4.0].

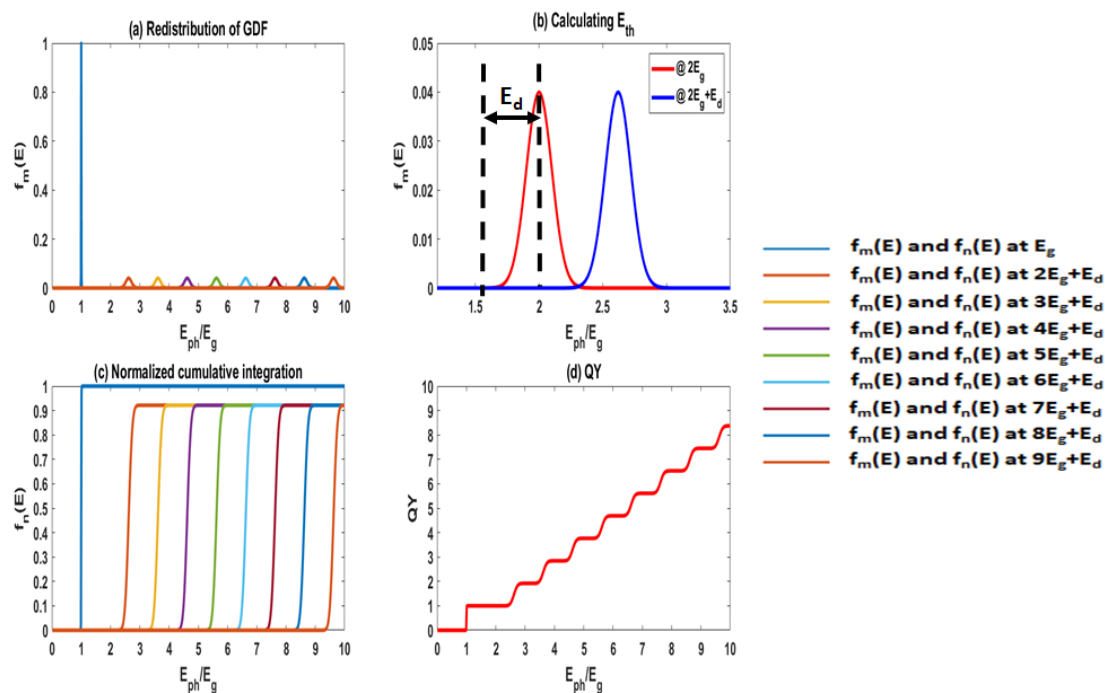


**Figure 2.** Conversion from the GDF to the NQY at  $\sigma_1 = 0.004$  at  $E_g$  and  $\sigma_m = 0.1$  at  $m \cdot E_g$  ( $m = 2, 3, 4, \dots$ ). (a) Normalized and redistributed GDF, (b) the corresponding GDF distribution for  $E_{th}$  calculation, (c) the results of Equation (7) representing the deviation from the ideal case, and (d) the corresponding QY. The units were normalized for (a,b) [Reprinted/Adapted from Ref. [39], 2021, Jongwon Lee, CC BY 4.0].

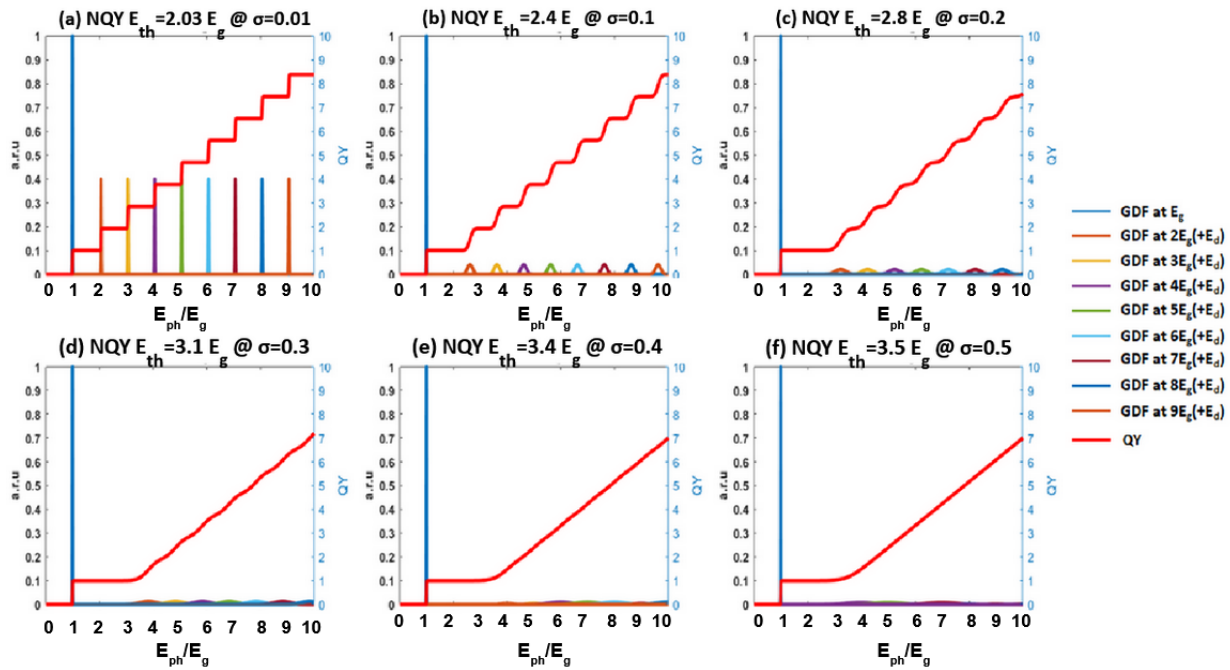


**Figure 3.** QY extraction from GDF distribution with variation of  $\sigma$ . From (a–f), we normalized the value of GDF to present the probability of carrier occupancy. The increase in  $\sigma$ , reduced the peak intensity and extended the width of GDF, which indicates increase in the low occupancy rate of carriers at each energy state and its threshold energy [Reprinted/Adapted from Ref. [39], 2021, Jongwon Lee, CC BY 4.0].

In addition, NQY involves the loss of carriers corresponding to each energy state owing to non-radiative recombination. To mathematically describe the NQY, we initially assumed that the generation of one EHP occurs at  $E_g$ , corresponding to the sharp peak ( $\sigma_1 = 4 \times 10^{-3}$ ) of the GDF. Following that, we chose  $\sigma_m = 0.1$  at  $m \cdot E_g$  ( $m = 2, 3, 4 \dots$ ) to account for the low occupancy of each energy state (Figure 2a, Equation (8)). As  $\sigma_m$  increases, the delta function lost its characteristics because the peak widens and decreases. In this study, we set the value  $\sigma_2 = 0.1$  to present non-radiative recombination such as ERE and  $f_C$  [1,30,31]. In this case, the ratio “peak intensity at  $2E_g$ /peak intensity at  $E_g$ ” was approximately 0.04, which represents the high non-radiative recombination rate of MEGSCs. To calculate the delayed  $E_{th}$ , a point corresponding to  $f(E) \geq 0$  at  $2E_g$ , on the left side of the GDF distribution ( $=E_d = 2E_g - x$ ), was selected (Figure 2b). We appended this point to  $m \cdot E_g$ ; therefore, the peaks redistributed at  $m \cdot E_g + E_d$ . Thus,  $\sigma$  modification represents a deviation from ideality, and its peak shift shows an adjusted point for the occupancy of carriers for MEG. It represents a higher photon energy ( $m \cdot E_g + E_d$ ) to excite the  $m^{th}$  exciton at  $m \cdot E_g$  and shifted  $E_{th}$  for the carrier multiplications.

$$f'_m(E) = [f_1(E), \frac{1}{\sigma_2 \sqrt{2\pi}} e^{-\frac{1}{2} \cdot (\frac{E - (2 \cdot E_g + E_d)}{\sigma_2})^2}, \dots, \frac{1}{\sigma \sqrt{2\pi}} e^{-\frac{1}{2} \cdot (\frac{E - (m \cdot E_g + E_d)}{\sigma_3})^2} \dots] / f_1(E), \quad (8)$$

$$\text{normalized } f'_m(E) = \left[ \frac{\sum_{i=1}^n \int_{E_i=0\text{eV}}^{x_n} f_1(E) dE}{\int_{E_i=0\text{eV}}^{E_f=10\text{eV}} f_1(E) dE}, \frac{\sum_{i=1}^n \int_{E_i=0\text{eV}}^{x_n} \frac{1}{\sigma_2 \sqrt{2\pi}} e^{-\frac{1}{2} \cdot (\frac{E - (2 \cdot E_g + E_d)}{\sigma_2})^2} dE}{\int_{E_i=0\text{eV}}^{E_f=10\text{eV}} f_1(E) dE}, \dots \right] \quad (9)$$

$$= \left[ \frac{\sum_{i=1}^n \int_{E_i=0\text{eV}}^{x_n} \frac{1}{\sigma_3 \sqrt{2\pi}} e^{-\frac{1}{2} \cdot (\frac{E - (m \cdot E_g + E_d)}{\sigma_3})^2} dE}{\int_{E_i=0\text{eV}}^{E_f=10\text{eV}} f_1(E) dE}, \dots \right]$$

$$NQY = \text{sum}(\text{normalized } f_m'(E)) \quad (10)$$

Further, we reorganized the DB of the MEGSC by adjusting the reverse saturation current density ( $J_0$ ) by including the non-radiative recombination ratio. In fact,  $f_{NR}$  represents the ratio of the radiative to non-radiative recombination rates. For this approach, we defined  $f_{NR}$  as the ratio of the maximum value of  $f_1(E_g)$  (for radiative recombination) to  $f_2'(2E_g + E_d)$  (for non-radiative recombination) to represent the status of radiative recombination while including the NR term, as given in Equations (11)–(16).

$$f_{NR} = \frac{\max(f_2(2E_g + E_d))}{\max(f_1(E_g))} = \frac{\max\left(\frac{1}{\sigma_2\sqrt{2\pi}}e^{-\frac{1}{2}\cdot\left(\frac{E-(2E_g+E_d)}{\sigma_2}\right)^2}\right)}{\max\left(\frac{1}{\sigma_1\sqrt{2\pi}}e^{-\frac{1}{2}\cdot\left(\frac{E-E_g}{\sigma_1}\right)^2}\right)} \quad (11)$$

$$\phi_{MEG}(E_1, E_2, T, \mu_{MEG}) = \frac{2\pi}{h^3 c^2} \int_{E_1}^{E_2} \frac{QY(E) \cdot E^2}{\exp[(E - \mu_{MEG})/kT] - 1} dE \quad (12)$$

$$J_{BB} = q \cdot C \cdot \phi_{MEG}(E_g, \infty, T_S, 0) + q \cdot C \cdot (1 - f_S) \cdot \phi_{MEG}(E_g, \infty, T_C, 0) - q \cdot \phi_{MEG}(E_g, \infty, T_S, \mu_{MEG}) \quad (13)$$

$$\mu_{MEG} = q \cdot QY(E) \cdot V \quad (14)$$

where  $\phi$  denotes the particle flux given by Planck's equation for temperature  $T$  with the chemical potential  $\mu$  in the photon energy range between  $E_1$  and  $E_2$ . In the above expressions,  $h$  denotes Planck's constant,  $c$  indicates the speed of light, and  $\mu$  denotes the CP of a single-junction solar cell ( $q \cdot V$ ) at the operating voltage  $V$ ,  $\mu_{MEG}$  denotes the CP of the MEG ( $q \cdot QY(E) \cdot V$ ),  $k$  denotes the Boltzmann constant,  $J$  corresponds to the current density of the solar cell,  $q$  denotes the charge,  $C$  indicates the optical concentration,  $f_S$  denotes the geometry factor ( $1/46,200$ ),  $T_S$  indicates the temperature of the sun ( $6000$  K), and  $T_C$  denotes the solar cell temperature ( $300$  K).

According to the DB limit theory [1,31], non-radiative and radiative generation and recombination should be conserved by controlling the non-radiative recombination ratio. The balanced equation is given by Equation (15), and its organized form is shown in Equation (16) [1,31].

$$F_{S,MEG} - F_{C,MEG}(V) + R_{MEG}(0) - R_{MEG}(V) - \frac{J_{BB}}{q} = 0, \quad (15)$$

where  $F_{S,MEG}$  and  $F_{C,MEG}(V)$  denote the generation and recombination for the radiative term, respectively, and  $R_{MEG}(0)$  and  $R_{MEG}(V)$  indicate non-radiative generation and recombination, respectively [31].

$$J_{BB} = q \cdot (F_{S,MEG} - F_{C0,MEG}) + q \cdot \left(\frac{F_{C0,MEG}}{f_{nr}}\right) [1 - \exp(q \cdot QY \cdot V / (k \cdot T_C))] \\ = q \cdot (F_{S,MEG} - F_{C0,MEG}) + J_0 \cdot [1 - \exp(q \cdot QY \cdot V / (k \cdot T_C))], \quad (16)$$

where  $F_{S,MEG} = C \cdot f_S \cdot \phi_{MEG}(E_g, \infty, T_S, 0) + C \cdot (1 - f_S) \cdot \phi_{MEG}(E_g, \infty, T_C, 0)$ ,  $F_{C0,MEG} = \phi_{MEG}(E_g, \infty, T_C, 0)$ .

Further,  $f_{NR} = 1$  describes the ideal condition of the MEGSC because it considers only radiative recombination. In addition,  $f_{NR}$  is inversely proportional to  $J_0$ . For instance,  $f_{NR} = 0.04$  means the increase in the ideal saturation current by 25 times of  $J_0$  because of the NR term and decrease in its theoretical efficiency. We discuss this in more detail in the Results section.

### 3. Results and Discussion

In this section, we discuss the variation in  $\sigma$  and the non-idealities of  $QY$  and its corresponding DB limit of MEGSC. In ideal nanostructured MEGSCs, the  $QY$  is given by



the staircase function because there are no carrier losses owing to the near-ideal material quality. However, most of the measurement data showed that QY exhibits a linear increase once  $E_{th}$  exceeds  $2E_g$  because of material defects (e.g., surface traps) [16–20]. Figure 3 presents the results of the QY calculations based on the GDF distribution (occupancy of carriers). When  $\sigma = 4 \times 10^{-3}$  for every energy state, the QY exhibited a staircase curve analogous to the IQY (Figure 1). However, as  $\sigma$  increases, the delta function started losing its characteristic shape owing to the loss of carriers in the zero-dimensional structures. In other words, the probability of the occupation of energy states by carriers decreased for every energy state. Therefore, this can be regarded as an effect of the delayed energy states. Finally, the QY plot exhibited linear shape with an increase in  $E_{th}$ . (Figure 3a–f). For instance, as shown in Figure 3, the QY shapes for  $\sigma = 0.01, 0.1$ , and  $0.2$  (Figure 3a–c) did not accurately correspond to a step function, and  $E_{th}$  was below  $3E_g$ . For  $\sigma = 0.3$  (Figure 3d),  $E_{th}$  equaled to  $3.1E_g$ , and the characteristic shape of the staircase function disappeared. Typically, for  $\sigma = 0.01$  (Figure 3a), the staircase step function existed; however, its maximum value of QY was less than 9 in the IQY case. Furthermore, for  $\sigma = 0.4$  and  $0.5$  (Figure 3e,f), QY increased linearly, exhibiting a slope slightly less than 1, and  $E_{th} = 3.4 - 3.5E_g$ . This indicates that MEGSCs' behavior changing to conventional single-junction solar cells was owed to increased  $E_{th}$ . Thus, the width and height of the peak of the GDF distribution for each energy state indicate the status of non-ideality, describing the characteristics of the delta function that relates to material imperfections in the nanostructures.

In other words, the IQY case entails a high possibility of carriers occupying the energy levels or maintaining a sharp peak for each energy state ( $m \cdot E_g$ ). In addition, the material quality of the nanostructure was maintained without carrier loss. However, NQY describes the imperfections of MEGSCs owing to NR, such as those arising from the occurrence of surface traps inside nanostructures [16–20]. The peak intensity exhibited by the GDF is a key parameter in determining the quality of the nanostructures. Except for the IQY case, the peaks (from  $2E_g$ ) indicated low carrier occupancies. For instance, when the highest peak at  $E_g$  corresponded to one, the second highest peak was below 0.04 (at  $\sigma = 0.1$ ). The intensity of the highest peak at  $E_g$  was approximately 25 times higher than that of the second-highest peak at  $2E_g$ , indicating that the carrier generation rate at  $m \cdot E_g$  was not sufficiently high owing to NR or material defects. This difference gives rise to a substantial reverse saturation current because of the increased non-radiative recombination rate, thereby degrading electrical parameters such as the open-circuit voltage and short-circuit current losses. Thus, the curve exhibited by QY starts losing its staircase shape; furthermore, it became linear owing to the carrier losses at each energy state. Therefore, the NR ratio increased.

To successfully demonstrate the advantages of the nanostructure in MEGSCs, the solar cell material should be nearly perfect with negligible non-radiative recombination to surpass the SQ limit. To verify the NR model in the DB, we tested the relationships between the Heaviside step and Dirac delta function in the DB limit (Equations (11)–(16)) under one sun illumination. We organized the simulation results in Figures 4 and 5, Tables 1 and 2 to compare the different cases of QYs. Without NR, the efficiency of the IQY case was nearly the same as that of the ideal MEGSC. For NQY without NR, the performance of the MEGSC approached to a conventional single-junction solar cell after  $E_{th} = 3E_g$ , whose calculated efficiency was same as the range of the SQ limit. However, after comparing the peak intensities by calculating  $f_{NR}$ , the overall efficiencies with NR were lower than the SQ limit, except for the case of  $\sigma = 0.01$ . For instance, the theoretical maximum efficiency at  $\sigma = 0.1$  was 34.5% without NR and 30.8% with NR, where  $J_0$  should be lower than 25 times that of  $J_0$  to maintain the performance of the MEGSC. Optimum bandgap with NR was 1.14 eV, which is nearly same as that of Si (Figure 4 and Table 1). In other words, while regarding MEGSC with NR, the basic requirement for generating MEG is that  $E_{th}$  should be lower than  $2.4 E_g$  with a corresponding bandgap energy of 1.14 eV. Furthermore, to compare the different slopes of NQY, we performed additional tests by doubling  $\sigma_1$ . In this case, except for  $\sigma = 0.01$ , all exhibited a negligible MEG effect, where the theoretical

efficiencies were below the SQ limit. Even if the calculated efficiency of NQY without NR at  $E_{th} = 3E_g$  was slightly higher than the SQ limit, its recombination term in the DB limit considered only the radiative recombination limit. Therefore, for a practical MEGSC with  $E_{th} = 3E_g$ , the efficiency could be lower than 31.8%, which is same as the conventional single-junction solar cells.

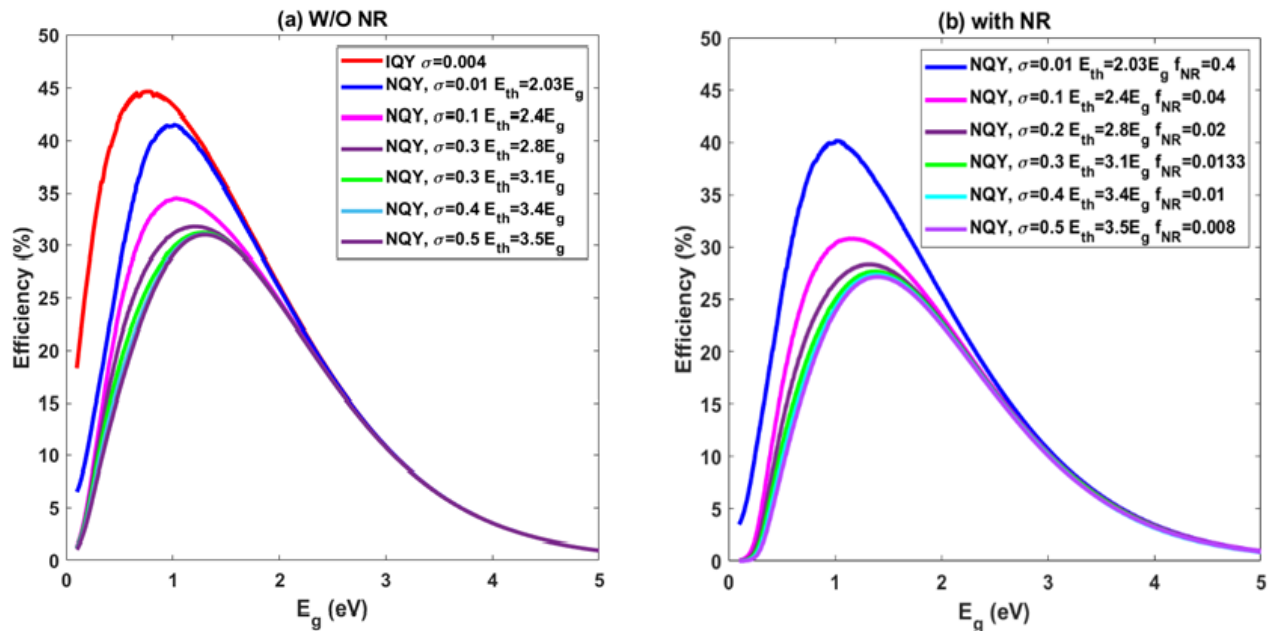


**Figure 4.** Efficiency vs.  $E_g$  after DB calculation with/without NR recombination impact under one sun illumination. The theoretical efficiencies saturated after  $\sigma = 0.4$  [Reprinted/Adapted from Ref. [39], 2021, Jongwon Lee, CC BY 4.0].

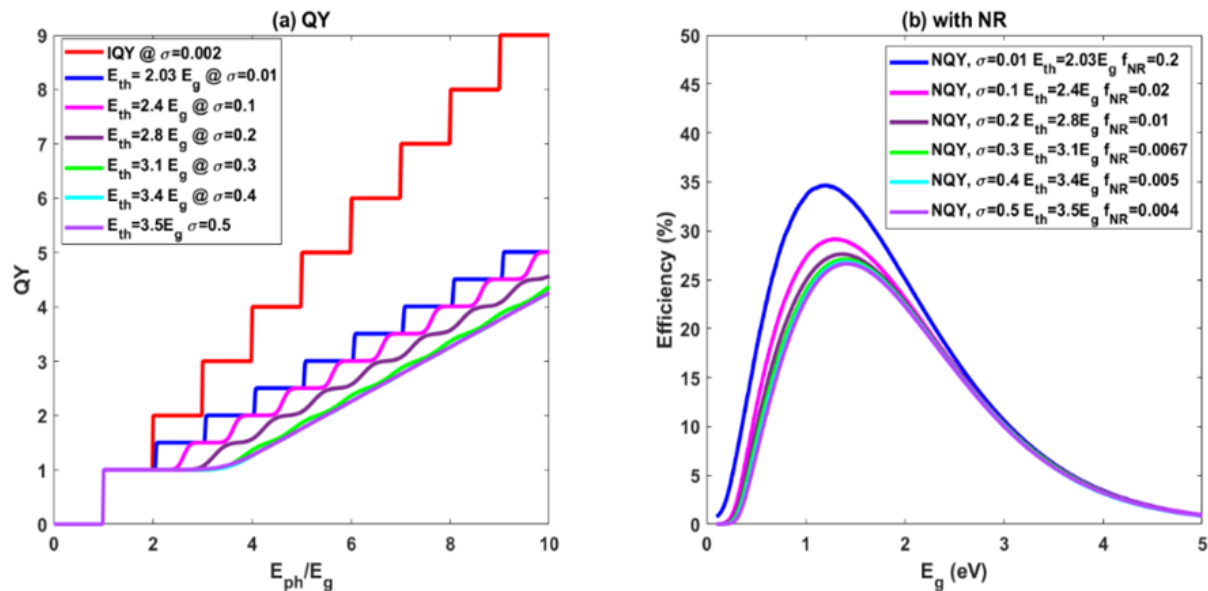


**Figure 5.**  $\sigma$  and its corresponding QY and its theoretical efficiency after DB calculation with NR impact under one sun illumination. Its maximum QY and its slopes are different than the case of  $\sigma_1 = 4 \times 10^{-3}$  [Reprinted/Adapted from Ref. [39], 2021, Jongwon Lee, CC BY 4.0].



**Table 1.** Optimum bandgaps and its maximum efficiencies with/without NR under one sun illumination, where  $\eta$  is efficiency [Reprinted/Adapted from Ref. [39], 2021, Jongwon Lee, CC BY 4.0].

	Without $f_{NR}$		With $f_{NR}$		
	$E_g$ (eV)	$\eta$ (%)	$f_{NR}$	$E_g$ (eV)	$\eta$ (%)
IQY ( $\sigma = 0.004$ )	0.77	44.6	N/A	N/A	N/A
$\sigma = 0.1, E_{th} = 2.03 E_g$	1.01	41.5	0.40	1.01	40.1
$\sigma = 0.1, E_{th} = 2.4 E_g$	1.03	34.5	0.040	1.14	30.8
$\sigma = 0.2, E_{th} = 2.8 E_g$	1.20	31.8	0.020	1.31	28.3
$\sigma = 0.3, E_{th} = 3.1 E_g$	1.28	31.2	0.0133	1.37	27.6
$\sigma = 0.4, E_{th} = 3.4 E_g$	1.30	31.0	0.01	1.39	27.3
$\sigma = 0.5, E_{th} = 3.5 E_g$	1.31	31.0	0.008	1.40	27.2

**Table 2.** Optimum bandgaps and its maximum efficiencies with NR under one sun illumination, where  $\eta$  is efficiency [Reprinted/Adapted from Ref. [39], 2021, Jongwon Lee, CC BY 4.0].

$\sigma_1 = 2 \times 10^{-3}$	With $f_{NR}$		
	$f_{NR}$	$E_g$ (eV)	$\eta$ (%)
$\sigma = 0.01, E_{th} = 2.03 E_g$	0.200	1.20	34.7
$\sigma = 0.1, E_{th} = 2.4 E_g$	0.020	1.30	29.1
$\sigma = 0.2, E_{th} = 2.8 E_g$	0.010	1.37	27.6
$\sigma = 0.3, E_{th} = 3.1 E_g$	0.0067	1.39	27.1
$\sigma = 0.4, E_{th} = 3.4 E_g$	0.005	1.41	26.8
$\sigma = 0.5, E_{th} = 3.5 E_g$	0.004	1.42	26.6

To compare the different slopes of NQY, we performed calculations with  $\sigma_1 = 2 \times 10^{-3}$  (Figure 5a,b, Table 2). For this simulation, after increasing  $\sigma$  twice, the corresponding slope at  $\sigma = 0.5$  was 0.49. This value was approximately 50% lower than that obtained for  $\sigma = 4 \times 10^{-3}$ . Except for  $\sigma_1 = 0.01$ , the other theoretical efficiencies were lower than 30%, which did not surpass the SQ limit (Figure 5b). In other words, even if the QY is greater than 100% after  $E_{th} = 2E_g$ , the MEGSC loses its performance owing to NR impact by the increased reverse saturation current densities. Only the  $E_{th} = 2.03E_g$  case provided the expected results of MEGSC, where  $E_{th}$  was nearly close to  $2E_g$  and its QY exhibited a staircase step function, although the value was not ideal.

#### 4. Conclusions

We devised a mathematical approach to extract QY based on GDF to discuss the ideality of MEGSCs. Through QY extraction analysis, we first mathematically identified the limitations arising from material imperfections in MEGSCs owing to non-idealities. Based on the delta function analysis, we employed the GDF to determine the impact of EHP generation for each energy state of a MEGSC and analyzed the variation in the shape of the GDF distribution, and this distribution was rearranged accordingly. Based on the variation and rearrangement of the GDF distribution, the QY can be theoretically determined. The difference between the GDF peak intensities of  $E_g$  and  $m \cdot E_g$  ( $m = 2, 3, 4 \dots$ ) can be employed to quantitatively analyze the occupancy of electrons at  $m \cdot E_g$  and the non-idealities of the MEGSCs. The large deviation from the ideal case appears due to an increase in the  $E_{th}$  and linearly increasing slope of the QY plot. Furthermore, non-idealities were explained based on the imperfections of the nanostructures. Notably, it is difficult to realize effective MEGSCs because of the imperfections, which results in NR or non-idealities. Moreover, we applied these results to the DB limit of the MEGSC with the NR term by calculating the ratio of radiative to non-radiative recombination. Considering this ratio, the overall efficiencies are lower than the SQ limit, and require  $E_{th}$  and optimum bandgaps lower than  $2.4E_g$  and 1.14 eV, respectively, to maintain the characteristics of MEGSC. Furthermore, to compare the different QY, we increased  $\sigma_1$  by two times, which reduced the maximum QY by approximately 50% and resulted in poor

theoretical performance. This suggests that the decrease in the slope of NQY results in a single-junction solar cell performance, even if QY increases slightly after  $E_{th}$  (slope of NQY is 0.49). This work: (1) is based on a mathematical approach that investigates the delta function and its deviation to evaluate QY,  $E_{th}$  and its corresponding theoretical efficiency, and (2) conceptually explains the dependency of materials. Due to the signal response of pump-probe measurement (impulse or step response), we could put forward the main idea of applying a Gaussian distribution and Heaviside step function for this study. Further studies are necessary to justify this approach by modifying the pump-probe measurement systems.

**Author Contributions:** Conceptualization, J.L.; methodology, J.L.; validation, J.L.; formal analysis, J.L. Investigation, J.L. Data curation, J.L. Writing—original draft preparation, J.L. Writing—Review and Editing, J.L. and C.-H.A.; supervision, C.-H.A. All authors have read and agreed to the published version of the manuscript.

**Funding:** This work is supported by the Education and Research Promotion Program of KOREATECH in 2021.

**Data Availability Statement:** The data presented in this study are openly available in arXiv:2101.01524v2 at <https://doi.org/10.48550/arXiv.2101.01525>, Ref [39].

**Conflicts of Interest:** The authors declare no conflict of interest.

## References

- Shockley, W.; Queisser, H.J. Detailed Balance Limit of Efficiency of p-n Junction Solar Cells. *J. Appl. Phys.* **1961**, *32*, 510–519. [\[CrossRef\]](#)
- Green, M.A. Third generation photovoltaics: Solar cells for 2020 and beyond. *Phys. E Low-Dimens. Syst. Nanostruct.* **2002**, *14*, 65–70. [\[CrossRef\]](#)
- Nozik, A.J. Quantum dot solar cells. *Phys. E Low-Dimens. Syst. Nanostruct.* **2002**, *14*, 115–120. [\[CrossRef\]](#)
- Luque, A.; Martí, A. Increasing the efficiency of ideal solar cells by photon induced transitions at intermediate levels. *Phys. Rev. Lett.* **1997**, *78*, 5014–5017. [\[CrossRef\]](#)
- Jacak, J.E.; Jacak, W.A. Routes for Metallization of Perovskite Solar Cells. *Materials* **2022**, *15*, 2254. [\[CrossRef\]](#)
- Kolodinski, S.; Werner, J.H.; Wittchen, T.; Queisser, H.J. Quantum efficiencies exceeding unity due to impact ionization in silicon solar cells. *Appl. Phys. Lett.* **1993**, *63*, 2405–2407. [\[CrossRef\]](#)
- Werner, J.H.; Kolodinski, S.; Queisser, H.J. Novel optimization principles and efficiency limits for semiconductor solar cells. *Phys. Rev. Lett.* **1994**, *72*, 3851–3854. [\[CrossRef\]](#)
- Werner, J.H.; Brendel, R.; Queisser, H.J. New upper efficiency limits for semiconductor solar cells. In Proceedings of the IEEE 1st World Conference on Photovoltaic Energy Conversion, Waikoloa, HI, USA, 5–9 December 1994; pp. 1742–1745.
- Werner, J.H.; Brendel, R.; Queisser, H.J. Radiative efficiency limit of terrestrial solar cells with internal carrier multiplication. *Appl. Phys. Lett.* **1995**, *67*, 1028–1030. [\[CrossRef\]](#)
- Brendel, R.; Werner, J.H.; Queisser, H.J. Thermodynamic efficiency limits for semiconductor solar cells with carrier multiplication. *Sol. Energy Mater. Sol. Cells* **1996**, *41–42*, 419–425. [\[CrossRef\]](#)
- De Vos, A.; Desoete, B. On the ideal performance of solar cells with larger-than-unity quantum efficiency. *Sol. Energy Mater. Sol. Cells* **1998**, *51*, 413–424. [\[CrossRef\]](#)
- Schaller, R.D.; Sykora, M.; Pietryga, J.M.; Klimov, V.I. Seven Excitons at a Cost of One: Redefining the limits for conversion efficiency of photons into charge carriers. *Nano Lett.* **2006**, *6*, 424–429. [\[CrossRef\]](#)
- Beard, M.C.; Ellingson, R.J. Multiple exciton generation in semiconductor nanocrystals: Toward efficient solar energy conversion. *Laser Photonics Rev.* **2008**, *2*, 377–399. [\[CrossRef\]](#)
- Kroupa, D.M.; Pach, G.F.; Vörös, M.; Giberti, F.; Chernomordik, B.D.; Crisp, R.W.; Nozik, A.J.; Johnson, J.C.; Singh, R.; Klimov, V.I.; et al. Enhanced Multiple Exciton Generation in PbS/CdS Janus-like Heterostructured Nanocrystals. *ACS Nano* **2018**, *12*, 10084–10094. [\[CrossRef\]](#)
- Marri, I.; Ossicini, S. Multiple exciton generation in isolated and interacting silicon nanocrystals. *Nanoscale* **2021**, *13*, 12119. [\[CrossRef\]](#) [\[PubMed\]](#)
- Jaeger, H.M.; Fischer, S.; Prezhdo, O.V. Decoherence-induced surface hopping. *J. Chem. Phys.* **2012**, *136*, 22A545. [\[CrossRef\]](#) [\[PubMed\]](#)
- Beard, M.C.; Midgett, A.G.; Law, M.; Semonin, O.E.; Ellingson, R.J.; Nozik, A.J. Variations in the quantum efficiency of multiple exciton generation for a series of chemically treated PbSe nanocrystal films. *Nano Lett.* **2009**, *9*, 836–845. [\[CrossRef\]](#) [\[PubMed\]](#)
- Ehrler, B.; Musselman, K.P.; Böhm, M.L.; Morgenstern, F.S.F.; Vaynzof, Y.; Walker, B.J.; MacManus-Driscoll, J.L.; Greenham, N.C. Preventing Interfacial Recombination in Colloidal Quantum Dot Solar Cells by Doping the Metal Oxide. *ACS Nano* **2013**, *7*, 4210–4220. [\[CrossRef\]](#) [\[PubMed\]](#)

19. Ip, A.H.; Thon, S.M.; Hoogland, S.; Voznyy, O.; Zhitomirsky, D.; Debnath, R.; Levina, L.; Rollny, L.R.; Carey, G.H.; Fischer, A.; et al. Hybrid passivated colloidal quantum dot solids. *Nat. Nanotechnol.* **2012**, *7*, 577–582. [CrossRef]
20. Li, H.; Zhitomirsky, D.; Dave, S.; Grossman, J.C. Toward the Ultimate Limit of Connectivity in Quantum Dots with High Mobility and Clean Gaps. *ACS Nano* **2016**, *10*, 606–614. [CrossRef]
21. Kershaw, S.V.; Rogach, A.L. Carrier Multiplication Mechanisms and Competing Processes in Colloidal Semiconductor Nanostructures. *Materials* **2017**, *10*, 1095. [CrossRef]
22. Beard, M.C. Multiple Exciton Generation in Semiconductor Quantum Dots. *J. Phys. Chem. Lett.* **2011**, *2*, 1282–1288. [CrossRef] [PubMed]
23. Nair, G.; Bawendi, M.C. Carrier multiplication yields of CdSe and CdTe nanocrystals by transient photoluminescence spectroscopy. *Phys. Rev. B* **2007**, *76*, 081304. [CrossRef]
24. Schaller, R.D.; Petruska, M.A.; Klimov, V.I. Effect of electronic structure on carrier multiplication efficiency: Comparative study of PbSe and CdSe nanocrystals. *Appl. Phys. Lett.* **2005**, *87*, 253102. [CrossRef]
25. Schaller, R.D.; Pietryga, J.M.; Klimov, V.I. Carrier multiplication in InAs nanocrystal quantum dots with an onset defined by the energy conservation limit. *Nano Lett.* **2007**, *7*, 3469–3476. [CrossRef]
26. Hanna, M.C.; Nozik, A.J. Solar conversion efficiency of photovoltaic and photoelectrolysis cells with carrier multiplication absorbers. *J. Appl. Phys.* **2006**, *100*, 074510. [CrossRef]
27. Klimov, V.I. Detailed-balance power conversion limits of nanocrystal-quantum-dot solar cells in the presence of carrier multiplication. *Appl. Phys. Lett.* **2006**, *89*, 123118. [CrossRef]
28. Su, W.A.; Shen, W.Z. A statistical exploration of multiple exciton generation in silicon quantum dots and optoelectronic application. *Appl. Phys. Lett.* **2012**, *100*, 071111. [CrossRef]
29. Hokins, R.F. (Ed.) Chapter 2—Delta Functions: Introduction to Generalized Functions. In *The Dirac Delta Function*, 2nd ed.; Woodhead Publishing: Sawston, UK, 2011; pp. 26–46, ISBN 9781904275398. [CrossRef]
30. Aliukov, S.; Alabugin, A.; Osintsev, K. Review of Methods, Applications and Publications on the Approximation of Piecewise Linear and Generalized Functions. *Mathematics* **2022**, *10*, 3023. [CrossRef]
31. Beard, M.C.; Johnson, J.C.; Luther, J.M.; Nozik, A.J. Multiple exciton generation in quantum dots versus singlet fission in molecular chromophores for solar photon conversion. *Philos. Trans. R. Soc. A Math. Phys. Eng. Sci.* **2015**, *373*, 20140412. [CrossRef]
32. Semonin, O.S.; Luther, J.; Choi, S.; Chen, H.-Y.; Gao, J.; Nozik, A.; Beard, M. Peak External Photocurrent Quantum Efficiency Exceeding 100% via MEG in a Quantum Dot Solar Cell. *Science* **2011**, *334*, 1530–1533. [CrossRef]
33. Davis, N.; Böhm, M.L.; Tabachnyk, M.; Wisnivesky-Rocca-Rivarola, F.; Jellicoe, T.C.; Ducati, C.; Ehrler, B.; Greenham, N.C. Multiple-exciton generation in lead selenide nanorod solar cells with external quantum efficiencies exceeding 120%. *Nat. Commun.* **2015**, *6*, 8259. [CrossRef]
34. Böhm, M.L.; Jellicoe, T.C.; Tabachnyk, M.; Davis, N.; Wisnivesky-Rocca-Rivarola, F.; Ducati, C.; Ehrler, B.; Bakulin, A.A.; Greenham, N.C. Lead Telluride Quantum Dot Solar Cells Displaying External Quantum Efficiencies Exceeding 120%. *Nano Lett.* **2015**, *15*, 7987–7993. [CrossRef] [PubMed]
35. Goodwin, H.; Jellicoe, T.; Davis, N.; Böhm, M. Multiple exciton generation in quantum dot-based solar cells. *Nanophotonics* **2018**, *7*, 111–126. [CrossRef]
36. Kurzweg, U.H. Available online: <https://mae.ufl.edu/uhk/HEAVISIDE.pdf> (accessed on 1 November 2020).
37. Zhu, L.; Lee, K.-H.; Yamaguchi, M.; Akiyama, H.; Kanemitsu, Y.; Araki, K.; Kojima, N. Analysis of nonradiative recombination in quantum dot solar cells and materials. *Prog. Photovolt. Res. Appl.* **2019**, *27*, 971–977. [CrossRef]
38. Lee, J.; Honsberg, C.B. Numerical Analysis of the Detailed Balance of Multiple Exciton Generation Solar Cells with Nonradiative Recombination. *Appl. Sci.* **2020**, *10*, 5558. [CrossRef]
39. Lee, J. Multiple Exciton Generation Solar Cells: Numerical Approaches of Quantum Yield Extraction and its Limiting Efficiencies. *arXiv* **2021**, arXiv:2101.01525.

**Disclaimer/Publisher’s Note:** The statements, opinions and data contained in all publications are solely those of the individual author(s) and contributor(s) and not of MDPI and/or the editor(s). MDPI and/or the editor(s) disclaim responsibility for any injury to people or property resulting from any ideas, methods, instructions or products referred to in the content.